Rapid Communication

Nanostructured free surfaces in plant-based plywoods driven by chiral capillarity

P. Rofouie [a], D. Pasini [b], Alejandro D. Rey [a],*

[a] Department of Chemical Engineering, McGill University, Montreal, Quebec H3A 2B2, Canada
[b] Department of Mechanical Engineering, McGill University, Montreal, Quebec H3A 2K6, Canada

ABSTRACT

Periodic nano-structured surfaces in Nature are responsible for functionalities such as iridescent colors observed in some flower petal surfaces that act as diffraction gratings. We present a theoretical scaling and computational analysis of the formation and structural characteristics of surface nano-wrinkling using the well-known cellulose chiral liquid crystals (LC) material model system that displays the twisted plywood architecture. Using a generalized LC shape equation here adapted to cholesteric free surfaces, we derive a model in terms of three capillary pressures whose solution is the ubiquitous periodic relief of plywood surfaces. The period and depth of the surface structure are shown to be dependent on the plywood's helical pitch. The ratio of amplitude to period of the surface undulation scales linearly with the anisotropic surface tension. These new findings can be used to characterize plant-based plywoods as well as to inspire the design of optical devices based on chirality-driven nano-wrinkling.

© 2014 Published by Elsevier B.V.

Biological materials, such as DNA in human cells [1], cellulose in plant cell walls, chitin in arthropods cuticles [2], and collagen in human compact bones [3], exhibit Bouligand's twisted plywood architecture [4], which is that of cholesteric liquid crystal (CLC), shown in Fig. 1a. The CLC is characterized by the helix axis $\mathbf{H}$, the pitch length p_o and handedness (sign of p_o), and the average fiber orientation $\mathbf{n}$ which is normal to $\mathbf{H}$. Directed chiral nematic liquid crystal (CLC) self-assembly is the formation mechanism of this structure, as demonstrated through defect generation phenomena [5].

The plywood architecture (PA) is responsible for several unique properties of biological materials [5], such as surface nano-structures observed in LC DNA [6], cellulose [7], and collagen [8]. The surface topography and defects in CLC materials can provide unique optical properties forming the basis for applications, such as sensors, actuators, and reflector [9]. The petals of many floral plants have remarkable optical properties, such as iridescence and a striking metallic appearance. Structural color in flowers, such as the iridescence exhibited by *Hibiscus trionum* and *Tulipa kaufmanniana* petals is determined by surface diffraction gratings that consist of ordered striations or ridges that form on the epidermal cells [10]. Although the formation of these striations during the development of the petals is not well-understood yet, it is

believed that cellulosic CLCs are responsible for plant surface nanostructures and iridescent colors. Several years ago, it was discovered that concentrated aqueous solutions of (hydroxypropyl) cellulose (HPC) displayed iridescent colors that changed with concentration and viewing angle [11]. Efforts have been made to trap the CLC structure in solid films to create colored iridescent films. Fernandes et al. fabricated iridescent solid cellulosic films with tunable mechanical and structural color properties, which mimic the structures found in the surface of "Queen of the Night" tulip petals, which display periodic striation of about 1.5 μm, responsible for the petals' iridescence [12]. They indicated that the formation and periodicity of the surface structure are governed by the CLC structure.

The formation of surface nanostructures in CLC interfaces is a complex phenomenon involving interfacial tension, surface anchoring energy, and LC Frank elasticity [5]. Although there are several works investigating the cholesteric surface structures by microscopy methods including atomic force microscopy (AFM) [13,14], the complementary theoretical analysis of CLC surface wrinkling is not complete. Meister et al. investigated the free surfaces of CLC resulting in linear texture through minimization of surface energy [15]. They showed that for strong and finite anchoring, the CLC is distorted near the surface, resulting in an interfacial region whose structure and dimensions are essentially controlled by the elastic energy and the helical pitch [15]. The director distributions in the distorted region coupled with anchoring energy create nano-scale undulations in the free surface.

* Corresponding author at: 3610 University Street, Montreal, QC H3A 0C5, Canada.
Tel.: +1 514 398 4196; fax: +1 514 398 6678.
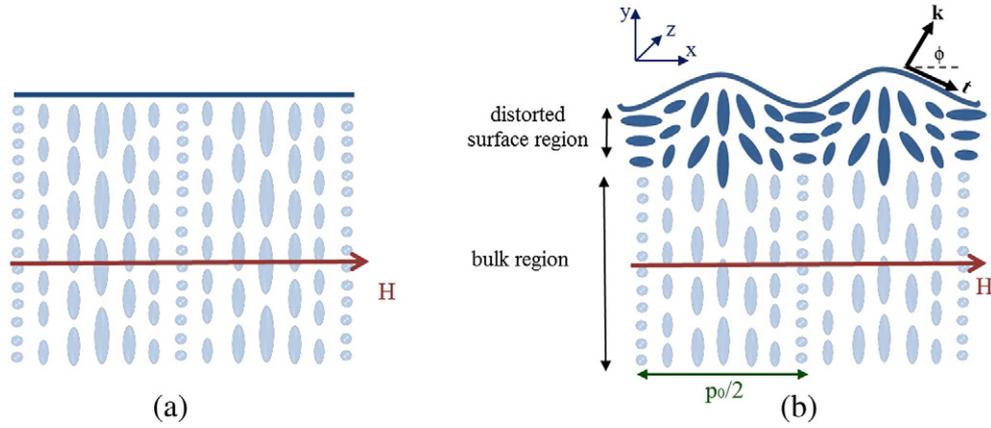E-mail address: alejandro.rey@mcgill.ca (A.D. Rey).

Fig. 1. Schematic of a cholesteric liquid crystal (plywood architecture) and surface structures. **H** is the helix unit vector, and p_o is the pitch. (a) The surface director has an ideal cholesteric twist and the surface is flat. (b) Bend and splay orientation distortions for $W < 0$ create surface undulations.
Adapted from [15].

The purpose of this communication is to contribute to the evolving understanding of nano-wrinkling in chiral surfaces. We focus on the cellulosic CLC material model [5]. We use the generalized shape equation for anisotropic interfaces using the Cahn–Hoffman capillarity vector developed for LCs [16] and the well-known Rapini–Papoular anchoring energy [17] for the anisotropic part of the interfacial tension, to analyze periodic nano-wrinkling in plant-based plywood free surfaces. The objective of this communication on chiral capillarity is to identify the key mechanisms that induce and resist nano-wrinkling in CLC, and to formulate nano-wrinkling scaling laws of biomimetic utility for the design of optical gratings and as a tool to characterize plant-based plywoods.

The CLC interfacial tension γ is given by the sum of the isotropic and anisotropic parts:

$$\gamma = \gamma_0 + \frac{W}{2}(\mathbf{n} \cdot \mathbf{k})^2 \tag{1}$$

where **k** is the surface unit normal and W is the anchoring energy; this is the Rapini–Papoular [17] equation. We restrict the discussion to homeotropic anchoring, because for planar surface anchoring ($W > 0$, $\mathbf{n.k} = 0$) the helicoidal structure, in which helix axis is perpendicular to the surface, will remain undistorted as it is the most stable and lowest energy state [18]; the undistorted helix results in a flat surface [15]. Since sufficiently strong homeotropic anchoring ($W < 0$) at the free surface is not compatible with the helix structures (helixes perpendicular ($\mathbf{H.k = 0}$) and parallel ($\mathbf{H.k} = 1$) to the surface); frustration leads to sub-surface defect nucleation. The appearance of defects in the bulk distorts the orientation in the CLC and results in a periodicity at the free surface whose wave length can vary from half helical pitch $p_0/2$ to p_0 or even greater [15,19]. Here we assume that the pitch of the distorted region is equal to the bulk p_0. The effect of $\mathbf{n}(x)$ on surface relief of two CLC structures is shown in Fig. 1. The distorted surface layer can be generated by either vertical nor tangential helixes in the bulk (only a horizontal helix alignment **H** is presented in Fig. 1).

To describe 1D surface undulations in a CLC we use a rectangular coordinate frame (x,y,z), where x is the undulation direction, and y is the vertical axis (Fig. 1). The amplitude of the vertical undulation is $h(x)$. For a 1D texture, the surface relief is constant in the z direction. The arc-length of the undulating surface is "s". The surface director field displaying planar splay-bend deformations is $\boldsymbol{n}(s) = (\cos qs, \sin qs, 0)$, where the wave-vector is $q = \frac{2\pi}{p_0}$; we only consider a right-handed helix ($q > 0$). The surface unit normal is $\boldsymbol{k}(s) = (\cos \phi, \sin \phi, 0)$ where $\phi(s)$ is the unknown normal angle to the surface. Using standard formulas, we re-express $(\mathbf{n,k})$ as a function of x instead of s.

We assume that the surface undulations in plant cell walls are formed through modulation in surface energy at the anisotropic-air interface and are influenced by the macroscopic chirality of the cellulose fiber. The coupling mechanism between the surface geometry and cellulose fiber orientation can be demonstrated through the shape equation. The formulation of the shape equation uses the capillary vector ξ [16]:

$$\boldsymbol{\xi} = \boldsymbol{\xi}_\perp + \boldsymbol{\xi}_\parallel; \; \boldsymbol{\xi}_\perp = \gamma\mathbf{k}; \; \boldsymbol{\xi}_\parallel = \mathbf{I}_s \cdot \frac{\partial\gamma}{\partial\mathbf{k}} \tag{2}$$

where $\mathbf{I}_s = \mathbf{I}\text{-}\mathbf{kk}$ is 2×2 unit surface dyadic. The anisotropic surface energy can change by dilation (change in area) and rotation (change in **k**); $\xi_\perp$ describes the increase of surface energy through dilation and $\xi_\parallel$ is the change in energy through rotation. For isotropic surfaces, $\xi_\parallel = 0$ and no rotational effects appear since $W = 0$. The total capillary pressure p_c that controls surface shape is [18]:

$$p_c = \nabla_s.\xi = \nabla_s.(\xi_\perp + \xi_\parallel) = \underbrace{\frac{\partial\xi_\perp}{\partial\mathbf{k}} : \nabla_s.\mathbf{k}}_{P_{\text{dilation}}: \text{ area dilation}} + \underbrace{\frac{\partial\xi_\parallel}{\partial\mathbf{k}} : \nabla_s.\mathbf{k}}_{P_{\text{rotation}}: \text{area rotation}} + \underbrace{\frac{\partial\xi_\parallel}{\partial\mathbf{n}} : \nabla_s.\mathbf{n}}_{P_{\text{director}}: \text{director curvature}} \tag{3}$$

where $\nabla_s = I_s. \nabla$ is the surface gradient. P_{dilation} is the usual Laplace pressure, P_{rotation} is the anisotropic pressure due to preferred orientation, and P_{director} is due to orientation gradients. As $h(x)$ is much smaller than the capillary length, gravitational energy is ignored. Using Eqs. (1)–(3) we obtain the total scaled capillary pressure [20]:

$$p_c = \left\{1 - \frac{B}{2}(\mathbf{n.k})^2 + B(\mathbf{n.t})^2\right\}\kappa - B\{(\mathbf{k.n})(\nabla_s.\mathbf{n}) + \mathbf{kn} : \nabla_s\mathbf{n}\} \tag{4}$$

where $B = W/\gamma_0$ is the scaled anchoring coefficient and $k = d\phi/ds$ is the surface curvature. The equation shows that the surface shape is the balance between tension and anchoring. The anchoring term is the driving force for surface undulations and it originates from the fact that this anisotropic surface energy is minimized when the director **n** is aligned along the preferred "easy axis". For a fixed cholesteric helical orientation, the only way to minimize this energy is to deform the interface to avoid energetically costly mismatch between the director and the easy axis. Since the director of a cholesteric is periodic, then the surface undulations are also periodic. When the director orientation deviates from the easy axis and the deviation generates gradients in surface tension, which are comparable to the characteristic kinetic energy density, the orientational-driven Marangoni flow may appear [21–23]; this flow mechanism is beyond the scope of this paper and will be explored in the future.

Setting $p_c = 0$ in Eq. (3) and using the above-specified splay-bend director $\mathbf{n}(s)$ and surface unit normal $\mathbf{k}(s)$ vectors give the governing nonlinear first order ODE for the normal angle $\varphi(x, B, p_0)$, where $-2 < B < 0$, $0 < p_0 < 100$ μm, $0 < x < L$. This ODE is solved using the well-known AUTO nonlinear software. The surface relief is then obtained from $h(x) = \int_0^L \cot\phi \, dx$. The boundary condition at $x = 0$, is $\phi|_{x=0} = \frac{\pi}{2}$. The three relevant outputs of the model are: (a) the generic features of the amplitude profile $h(x)$, (b) its maximum value h_{max}, and (c) its periodicity $h(x) = h(x + P)$. The two significant parameters influencing $h(x)$ are the scaled anchoring coefficient B (usually $-0.1 < B < 0$ or weak anisotropy) and the micron scale length of the pitch p_0.

Fig. 2 shows the computed normal angle profile $\phi(x)$ and the corresponding surface reliefs $h(x)$ for different B. The model predicts that the periodicity of surface relief equals to the pitch, p_0 and that h_{max} is few nm, consistent with the experimental findings [14,24]. Increasing anchoring (B) results in higher amplitudes. Decreasing chirality (increasing p_0) has a similar effect on h_{max}.

Using a standard order of magnitude analysis based on Eq. (3), we find a revealing close form expression for h_{max} as a function of anchoring (B) and chirality (p_0):

$$h_{max} = \frac{Bp_0}{1 + \delta B}. \tag{5}$$

The numerical results indicate that $\delta = 10.71 B^{-1.02}$. The prediction is that the ratio of amplitude/periodicity is essentially a linear function of the scaled anchoring B: $h_{max}/p_0 = 0.085B$. Since the value of B for the interface between the nematic and the isotropic phase/air usually is in the range $-0.1 < B < -0.01$, the estimated amplitude of surface undulation is about 1% of the undulation wavelength. The theoretical estimate, based on the shape equation, of the depth-to-period ratio is consistent with the experimental finding of CLC surfaces [14,24].

Next we shed light on the mechanisms behind chiral wrinkling using the three pressures. Fig. 3 shows the three surface pressures (Eq. (3)) as a function of "x". $P_{rotation}$ is an order of magnitude smaller than $P_{dilation}$ and $P_{director}$. The figure demonstrates that the main driving force is $P_{rotation}$ and that the resistance is the usual Laplace pressure $P_{dilation}$ (increasing energy with increasing area). Chiral capillarity acts through the spatially periodic director pressure $P_{director}$ to wrinkle the surface.

When the periodicity of the surface undulations is of the same order of the incident light wavelength, the structure has the potential to generate iridescence and colors through the diffraction grating mechanism. Structural color in floral plants originates mainly from ordered surface diffraction gratings that scatter incident light in the plane perpendicular
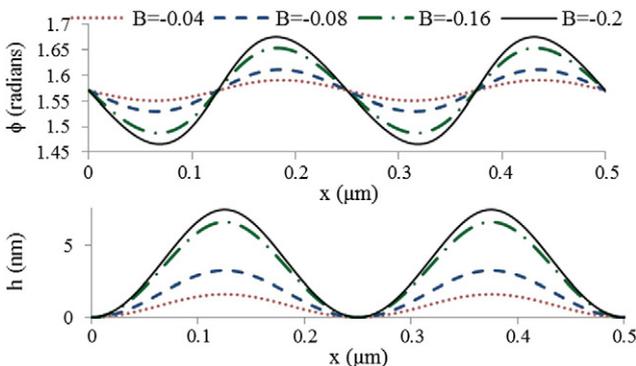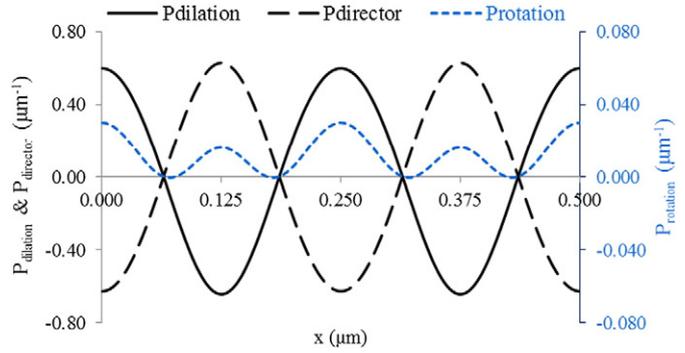

Fig. 3. The three capillary pressure ($P_{dilation}$, $P_{rotation}$, and $P_{director}$) profiles for B $= -0.05$ and $p_0 = 0.5$ μm.

to the direction of the periodic undulations according to the grating equation [25]:

$$m\lambda = \frac{p_0}{2}(sin\theta_i - sin\theta_d) \tag{7}$$

where θ_i and θ_d are angles of incidence and diffraction which govern the angular locations of the principal intensity maxima for the diffracted incident light with wavelength, λ, and m is the diffraction order. According to Eq. (7), for any given value of the angle of incidence θ_i, each wavelength λ scatters into different angular directions. When the incidence light is white light, different colors disperse in the perpendicular direction of the periodic structure, making the surface iridescent. Hence Eqs. (5) and (7) provide an important new relation between functionality and structure.

In summary, in this communication we have elucidated the main mechanisms that operate in chiral capillarity using plant-based plywoods as a model system. The plywood architecture found in many biological materials [3] is a CLC analogue with micron-range pitch. The essential feature of chiral capillarity is the interaction of anisotropy (director $\mathbf{n}$ of fibers), micron-range chirality (p_0), helix direction ($\mathbf{H}$) and free surface topography. When the cholesteric helix is parallel to a flat surface, frustration driven by the unavoidable (due to periodic $\mathbf{n}$) presence of high surface energy drives the surface uncoiling of the helix and the periodic tilting of the interface. This is another example of pattern formation by frustration, ubiquitous in mesophases [5]. A unique feature of liquid crystal surfaces [16] is the presence of Laplace pressure (area dilation), Herring's pressure (area rotation), and director orientation gradient pressure, as revealed succinctly by the surface gradient of the capillary vector ξ. Herring's pressure forms the basis of anisotropic crystal morphologies [16] and is included here as $P_{rotation}$. As the Herring's pressure depends on curvature, it is only the orientation pressure $P_{director}$ that wrinkles the surface with a wavelength that reflects the periodicity of the director filed. The amplitude of the surface relief is in the order of few nm and the wave-length is in order of μm. The ratio of amplitude/period is estimated by $0.085 \times W/\gamma_0$, which is consistent with the experimental values. Diffraction gratings generated by chiral capillarity can be used for the characterization of plant-based plywoods and for Nature-inspired optical devices. Since the pitch p_0 is sensitive to temperature, solvents, pH, and external fields we expect new functional material surfaces that operate through the chiral capillarity mechanism described here.

Fig. 2. Computed normal angle $\phi(x)$ and surface relief h(x) for $p_0 = 0.5$ μm and B $= -0.04, -0.08, -0.16$, and -0.2.

References

[1] F. Livolant, A. Leforestier, Condensed phases of DNA: structures and phase transitions, Prog. Polym. Sci. 21 (1996) 1115–1164.
[2] A.C. Neville, Biology of Fibrous Composites: Development Beyond the cell Membrane, Cambridge University Press, New York, NY, USA, 1993.
[3] M.M. Giraud Guille, Twisted plywood architecture of collagen fibrils in human compact-bone osteons, Calcif. Tissue Int. 42 (1988) 167–180.
[4] Y. Bouligand, Twisted fibrous arrangements in biological-materials and cholesteric mesophases, Tissue Cell 4 (1972) 189–217.
[5] A.D. Rey, Liquid crystal models of biological materials and processes, Soft Matter 6 (2010) 3402–3429.
[6] I.I. Smalyukh, O.V. Zribi, J.C. Butler, O.D. Lavrentovich, G.C.L. Wong, Structure and dynamics of liquid crystalline pattern formation in drying droplets of DNA, Phys. Rev. Lett. 96 (177801) (2006).
[7] A.F. Miller, A.M. Donald, Imaging of anisotropic cellulose suspensions using environmental scanning electron microscopy, Biomacromolecules 4 (2003) 510–517.
[8] J.E. Kirkwood, G.G. Fuller, Liquid crystalline collagen: a self-assembled morphology for the orientation of mammalian cells, Langmuir 25 (2009) 3200–3206.
[9] G. Agez, R. Bitar, M. Mitov, Color selectivity lent to a cholesteric liquid crystal by monitoring interface-induced deformations, Soft Matter 7 (2011) 2841–2847.
[10] H.M. Whitney, M. Kolle, P. Andrew, L. Chittka, U. Steiner, B.J. Glover, Floral iridescence, produced by diffractive optics, acts as a cue for animal pollinators, Science 323 (2009) 130–133.
[11] R.S. Werbowyj, D.G. Gray, Liquid–crystalline structure in aqueous hydroxypropyl cellulose solutions, Mol. Cryst. Liq. Cryst. 34 (1976) 97–103.
[12] S.N. Fernandes, Y. Geng, S. Vignolini, B.J. Glover, A.C. Trindade, J.P. Canejo, et al., Structural color and iridescence in transparent sheared cellulosic films, Macromol. Chem. Phys. 214 (2013) 25–32.
[13] B.D. Terris, R.J. Twieg, C. Nguyen, G. Sigaud, H.T. Nguyen, Force microscopy of chiral liquid–crystal surfaces, Europhys. Lett. 19 (1992) 85–90.
[14] P.E. Cladis, M. Kleman, Cholesteric domain texture, Mol. Cryst. Liq. Cryst. 16 (1972) 1–20.
[15] R. Meister, H. Dumoulin, M.A. Halle, P. Pieranski, Anchoring of a cholesteric liquid crystal at the free surface, J. Phys. II 6 (1996) 827–844.
[16] A.G. Cheong, A.D. Rey, Cahn–Hoffman capillarity vector thermodynamics for curved liquid crystal interfaces with applications to fiber instabilities, J. Chem. Phys. 117 (2002) 5062–5071.
[17] A. Rapini, M. Papoular, Distorsion d'une lamelle nématique sous champ magnétique conditions d'ancrage aux parois, J. Phys. Paris Colloques. 30 (1969) 54–56.
[18] B.I. Outram, S.J. Elston, Spontaneous and stable uniform lying helix liquid–crystal alignment, J. Appl. Phys. 113 (043103) (2013).
[19] A. Saupe, Disclinations and properties of director field in nematic and cholesteric liquid–crystals, Mol. Cryst. Liq. Cryst. 21 (1973) 211–238.
[20] A.D. Rey, Mechanical model for anisotropic curved interfaces with applications to surfactant-laden liquid–liquid crystal interfaces, Langmuir 22 (2006) 219–228.
[21] A.D. Rey, Nemato-capillarity theory and the orientation-induced Marangoni flow, Liq. Cryst. 26 (1999) 913–917.
[22] A.D. Rey, Marangoni flow in liquid crystal interfaces, J. Chem. Phys. 110 (1999) 9769–9770.
[23] R. Eelkema, M.M. Pollard, N. Katsonis, J. Vicario, D.J. Broer, B.L. Feringa, Rotational reorganization of doped cholesteric liquid crystalline films, J. Am. Chem. Soc. 128 (2006) 14397–14407.
[24] A. Boudet, M. Mitov, C. Bourgerette, T. Ondarcuhu, R. Coratger, Glassy cholesteric structure: thickness variation induced by electron radiation in transmission electron microscopy investigated by atomic force microscopy, Ultramicroscopy 88 (2001) 219–229.
[25] S. Vignolini, E. Moyroud, B.J. Glover, U. Steiner, Analysing photonic structures in plants, J. R. Soc. Interface 10 (20130394) (2013).